Fifth International Symposium on Marine Propulsors
smp'17, Espoo, Finland, June 2017

Long Tunnel Configurations for High Efficiency Thrusters

Stefano Brizzolara[1] & Enrico Bruno Brizzolara[2]

[1]Kevin T. Crofton Department of Aerospace and Ocean Engineering, Virginia Tech, Blacksburg, VA, USA
[2]Naval Architect and Marine Engineer, Independent Consultant, Genoa, Italy

ABSTRACT

The principal characteristics and hydrodynamic principles of a new type of tunnel configuration designed to improve the efficiency of long tunnel thrusters are presented. The proposed tunnel configuration is composed of three sections: a mid-section, having a smaller diameter, where the impeller is running and two end-sections having a larger diameter and transition piece. The hydrodynamic advantages of the new technology are introduced by first principles and then verified by a series of CFD calculations, allowing detailed analysis of the flow field. According current practice, installations with tunnel length/diameter ratios greater than four are deliberately avoided, resulting in oversized impeller designs. For a given tunnel length, the new proposed configuration, allows to design a smaller impeller which can meet and overcome the efficiency of a larger impeller having the ideal length/diameter ratio of 2~3. A series of alternative configurations of the new proposed technology are modeled and predicted thrust and efficiency are discussed.

Keywords

Tunnel thrusters, efficiency, CFD, ducted propellers.

1 INTRODUCTION

Tunnel Thrusters are very commonly used for station keeping and low speed maneuvering in the bow and stern of different types of vessels: from large ships to yachts and working boats, from offshore floating platforms to considerably smaller autonomous underwater vehicles. In spite of their wide diffusion, the design of tunnel system and its integration with the hull is still very empirical and based on limited scientifically proven/verified data. In fact, few systematic data have been published about the how the tunnel geometric particulars may influence the performance of the whole system, composed by the impeller and duct system.

The extensive experimental systematic study conducted by Mitsubishi (Taniguchi et al., 1966) remains one of the main source of experimental data to estimate the effect of different tunnel geometrical features, such as duct walls inclination, convergent and divergent tunnel ends and tunnel-end-wall fairings. The tests, though, regarded only a limited number of geometrical variation of the tunnel geometry. For instance, the maximum investigated tunnel length to impeller diameter ratio is L_D/D=3 and the tunnel geometry investigation were done with a single fixed pitch impeller geometry with a zero chord at tip, while most modern thrusters use a Kaplan-like propeller with finite (often maximum) chord at tip.

Figure 1 - Example of long bow tunnel thruster on a tanker

The importance of tunnel-end-wall fairing design in terms of thrust augmentation was remarked by Ridley (1969) on an actual bow thruster design for a bulk carrier, tested with six different fairings. 16% thrust increase was achieved by using rounded tunnel-end-wall fillet radius r_f =0.2D with respect to a right angle connection, at the same absorbed power; 10% thrust augmentation factor was achieved with conical fairing having 30deg average opening angle. A comprehensive review of the duct design features was given by Beveridge (1972), who added some interesting data and new theoretical insight on the maximum ideal efficiency attainable by ducted propellers, with and without end diffusers.

Not much has been added to the state of the art in the field since then. Moreover, all referenced experimental data are relative to model scale. RANSE simulations have demonstrated excellent accuracy (Yu and Yang, 2016) and offer a unique opportunity to perform full scale parametric predictions and investigations, overcoming the inherent limitations of potential flow based methods, which are valid tools for the design and analysis of the impeller (e.g. Gaggero et al. 2009), but inappropriate to deal with viscous flow physics that are primarily ruling the hydrodynamic design of the duct.

From a design standpoint, tunnel thruster installations may considerably differ in lengths, depending on the type of hull and the location. This paper addresses installations with long tunnel lengths L relative to the impeller diameter D, i.e. L/D≥4, as in the example of Figure 1. As it will be demonstrated, these types of installations are not so uncommon and could be actually greater in number, since often configuration with large L/D are deliberately discarded in order to avoid the distributed losses in the long tunnel. As a result, in ships with blunt bows, either large tunnel and propeller diameters are used (with a general increase of costs) or the location of the tunnel is moved extremely close to the bottom or extreme bow with a consequent loss of efficiency due to edge effects.

2 STEPPED LONG TUNNEL CONFIGURATION

Current design of tunnel thrusters and ducted propellers is based on constant or continuously varying diameter of the internal duct surface. According Brizzolara & Brizzolara (2016) a new tunnel configuration that features a diameter step (Figure 2) in introduced, in such a way that the internal surfaces are composed of three sections: a mid section (*tunnel*), having a smaller diameter D and a given length L_T, where the impeller is located, and two symmetric end sections (*in.large* & *out.large*) having a length L_L and a larger diameter D_L. The stepped connection between the center and end sections can vary in topological shape, from a simple sharp step (Figure 2) to conical or rounded step connections (Figure 3) of adequate proportions: defined by the slope angle α_s in the first case and by the ellipticity factor in the latter.

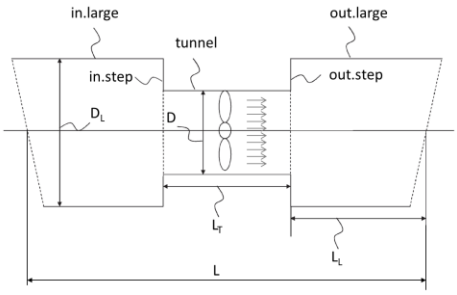

Figure 2 – New Stepped Long Tunnel Thruster configuration schematic drawing (Brizzolara & Brizzolara, 2016)

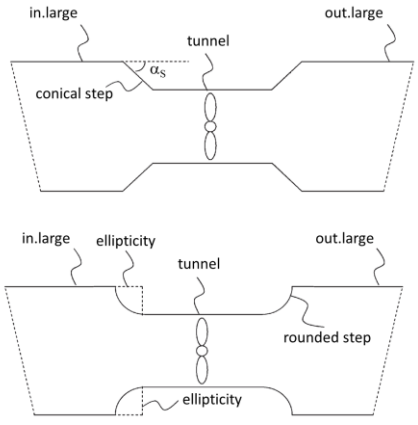

Figure 3 - Alternative duct inner step shapes: conical (top) and rounded (bottom)

The new particular design of the internal tunnel surfaces derives from the necessity to hydrodynamically decouple the mid-section, where the impeller is operating, from the rest of the long tunnel. A sudden increase of diameter between the mid and end sections, executed with a stepped connection piece, is desirable in order to trigger the separation of the jet flow exiting from the mid-section and entering in the outer section, in the intent of reducing friction losses in the outer tunnel section. Clearly the sharp step of the outflow (*out.step*) in Figure 2, will do the job, but its symmetric image (*in.step*), at the connection with the inflow conduit, is expected to create considerable concentrated losses. The balance between the gains and losses depends on the particular geometry and operating conditions.

The concentrated losses created at the *in.step* can be reduced by a conical connection (top sketch in Figure 3) and eventually reduced to a minimum value by an rounded connection (bottom in Figure 3), with opportune ellipticity factor, traded from the best design practice of hydraulic engineering. Both conical and blunt rounded step designs should be opportunely designed to maintain separation of the jet flow, at the outlet (*out.step*) side of the inner tunnel.

The hydrodynamic principles behind the proposed configuration will be better explained based on the findings of section 5 illustrating CFD results on the systematic series of geometric variation described in the next section. Details of numerical and physics modeling are given in section 4.

3 SYSTEMATIC GEOMETRY VARIATIONS

To characterize the hydrodynamics of the stepped tunnel configuration a series of geometrical variations has been generated and analyzed with a RANSE solver.

A reduced set of design variants is discussed in this paper for sake of brevity. This series is the -OS series that features a sharp connection between the tunnel end and the upstream (in-wall) and downstream (out-wall) duct sides, modelled as infinite span walls. The designs are visually presented with main dimensions in Figure 4.

The first two cases are straight constant diameter (D=0.8m) tunnels with two significantly different lengths, resulting in L/D=7.285 and L/D=1.5. They are named SLTT1-OS and SLTT1-short-OS, respectively.

The next four designs variants, SLTT2, share the same step in diameter of the duct, namely D_L/D = 1.375. Two of them feature a conical (*step -V*) connection between the mid-section and the end-sections. In the other two designs, the step in diameter is achieved through a rounded connection (*step -E*). For each different step typology, two mid-section lengths have been considered: L_T/D=1.5 (*suffix-S-*) and L_T/D=3 (*suffix–M-*).

Finally, other four designs were generated with a larger step height, corresponding to D_L/D = 2.0. These cases are named SLTT4. Three of them feature the same mid-section length (*-M-*) L_T/D=3 and implement the rounded (*-E*),

conical (-*V*) and right angle (-S) steps. Last case SLTT4S-S -OS features a square step too, but a shorter mid-section length L_T/D=1.5.

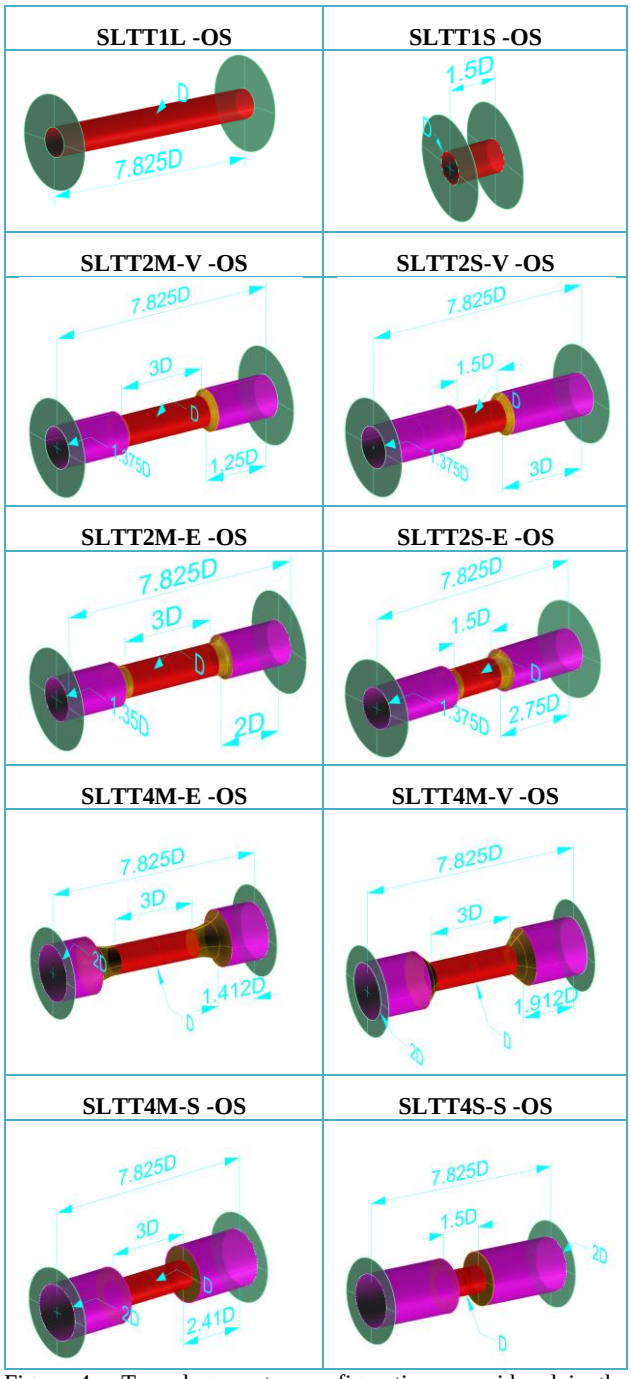

Figure 4 - Tunnel geometry configurations considered in the parametric CFD investigation. Only a circular portion of the upstream and downstream infinite side-walls are represented.

4 PHYSICS AND NUMERICAL MODELLING

The focus of this investigation is in the comparison of the viscous hydrodynamics of different duct designs. To the scope, a state of the art Reynolds-Averaged Navier-Stokes Equation (RANSE) solver has been used (StarCCM+, v.11), widely validated on different propeller flow analyses in steady and unsteady conditions (e.g. Brizzolara et al., 2008). The finite volume solver implementation for steady incompressible flows over unstructured polyhedral meshes was selected. This solver uses the SIMPLE method to conjugate pressure and velocity during the implicit solution of the RANSE equations, by means of an AMG accelerated algorithm. A two layers (Rody, 1991), shear driven, realizable k-ε turbulence model was preferred versus more sophisticated Reynolds stress transport models due to its robustness and good level of accuracy, also in separated flows, that does not require high density meshes to resolve the viscous sublayer. A second order scheme is used to discretize the convective term of the turbulence model.

Again, being the attention on duct hydrodynamics, a simplified axial and rotational actuator disk model is used to represent the hydrodynamic action of the impeller without the need of solving the flow around the blades (Villa et al., 2008). The actuator disk is located in place of the impeller (disk in the middle of Figure 7) and it imparts a non-uniform axial and tangential momentum to the flow passing through the occupied cells. Axial and tangential momentum sources vary along the radial coordinate according Goldstein's optimum distribution, according:

$$G(r') = r'\sqrt{1-r'} \qquad (1)$$

where $r'=r/R$ is the radial coordinate, running from the hub to the tip, normalized by the disk radius $R=D/2$. The same shape function G is used to distribute both the axial and rotational (tangential) momentum components. The shape function G multiplies by a proper scale factor in order to verify the equivalence between the total axial momentum imparted to the flow and the impeller thrust; and another scale factor in order to verify the equivalence between the total rotational momentum and the impeller torque.

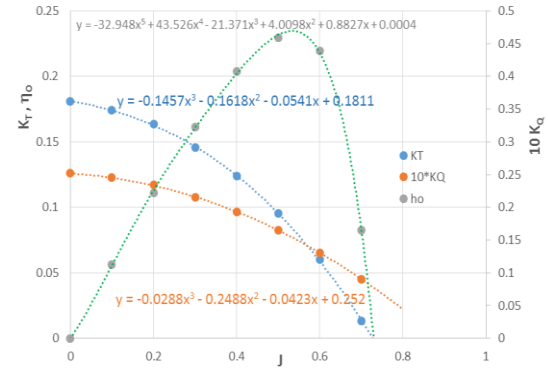

Figure 5 - Thrust torque and efficiency coefficients for the Ka-4-70 propeller considered in this study. Polynomial curve regression of each curve is given in the graph.

Impeller thrust $K_T=T/\rho n^2D^4$ and torque $K_Q=/\rho n^2D^5$ coefficients are specified as a function of the advance ratio $J=V_a/nD$, where n is the impeller rotational speed, D is the impeller diameter and V_a is the average inflow speed. In this study, a the hydrodynamic characteristics of a Ka-4-70 impeller operating in a circular cylinder have been derived from the experimental data of Van Manen & Oosterveld (1966), as presented in Figure 5. The calculation of the impeller inflow speed V_a is obtained by averaging the axial speed component in each cell passing through a control plane upstream of the actuator disk, at each implicit solver

iteration. It is verified that the dynamic characteristics of the actuator disk rapidly converge during the time the flow field builds up and reach the steady state inside the tunnel.

Domain topology and global dimensions are presented in Figure 6. On each side of the tunnel thruster, a cubic domain measuring ~37·D on its side is considered. A smooth-wall boundary condition is set on the two inner wall of the upstream (*in-wall*) and downstream (*out-wall*) domains. The rest of the upstream domain boundaries are set to stagnation-inlet. All downstream domain boundaries except the inner wall are set to pressure outlet.

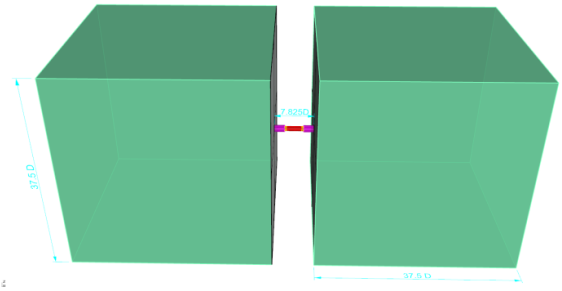

Figure 6 – CFD domain toplogy and size. The tunnel thruster measuring L=7.825·D is located in the middle of the two cubic upstream and downstream domains.

The six different parts composing the long stepped tunnel – namely *tunnel*, *in/out.large*, *in/out.step* – are modelled as smooth-wall distinct surfaces, to allow for individual integration of pressure and friction forces. Hence, the total pressure of the duct system is obtained by integrating pressure and friction forces on the two vertical walls (in and out wall) and on the entire inner surfaces of the duct.

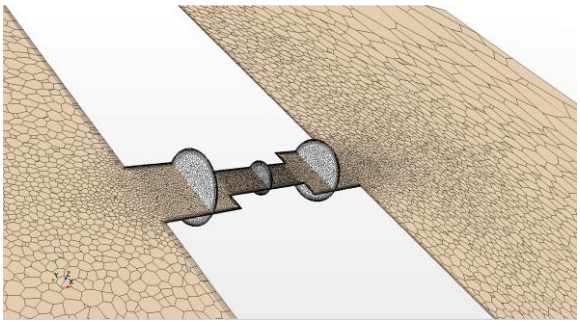

Figure 7 - Example of unstructured polyhedral mesh (500k cells) used for the CFD simulations. The case is SLTT4-medium-OS.

A typical mesh resolution, counting about 500k cells, used throughout this study, is presented in the view of Figure 7. Prismatic cells are used close to the wall boundaries, while polyhedral cells are used in the rest of the domain with density refinements inside the long stepped tunnel and around the upstream and downstream openings.

5 RESULTS

For the comparative analysis of the CFD results, the long straight tunnel thruster SLTT1 is taken as reference case. An impeller diameter D=0.8m and a given impeller thrust Tp=12kN are assumed. The preliminary thruster sizing study indicates that a Ka-4-70 impeller in a conventional (L/D=2~3) tunnel thruster would require an input power of about 190kW, at about 810 rpm. On this basis, the alternative designs listed in Figure 3 were generated and their hydrodynamic characteristics predicted by the RANSE solver are compared in this section. The same impeller (Ka-4-70) is considered for all different ducted configurations, presented in Figure 4 and the rotational speed necessary to achieve the same delivered impeller thrust (12kN) is found as part of the CFD solution. Alternative bases for comparison are possible, as for instance to consider a given impeller speed (allowing for different impeller thrust and torque values between different cases), or a given delivered power (also allowing for different impeller speed and thrust values). A more sophisticated comparison would consider the impeller pitch as an additional degree of freedom, in order to achieve the same rotational speed and power requested by the impeller in all cases, or the best efficiency at the given thrust.

In fact, in the comparison with equal impeller thrust, the different considered duct configurations imply different distributed and concentrated losses along the duct and consequently a different flow rate and a different thrust delivered by the duct. The total thrust *Ttot*, as presented in Figure 8, is then obtained by summation of the given impeller thrust Tp=12kN (constant) with the duct thrust *Td* found by CFD simulation for each alternative design.

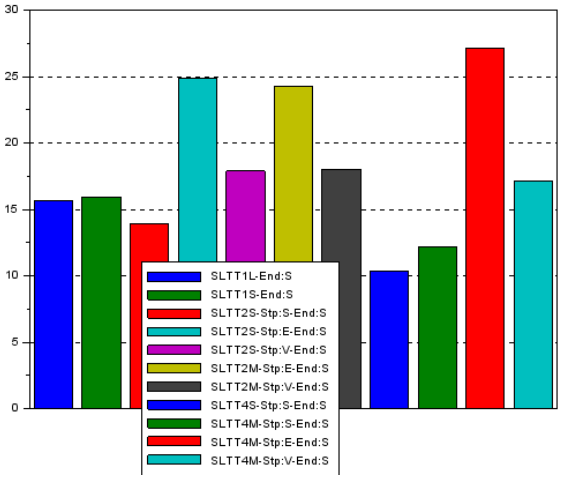

Figure 8 - Total Thrust *Ttot* [kN] predicted by the CFD model for the SLTT listed in Figure 4.

As it can be noted, considerable relative differences are predicted among the total thrust prediction of Figure 8. The predicted total thrust must be analyzed together with the predicted impeller speed (Figure 9) and the impeller torque (Figure 10) for a complete picture. For instance, the total thrust of the conventional tunnel thruster is higher for the configuration with a short tunnel (SLTT1-S), than a long tunnel (SLLT1-L). At the same time, the shorter conventional tunnel thruster also requires a lower input torque. These two effects combined ultimately mean an increased efficiency for SLTT1-S with respect to SLTT1-L, as can be noted in Figure 12. This was expected due to the higher friction losses in the longer tunnel and follows the trends found by Taniguchi et al. (1966), further explained by Beveridge (1972).

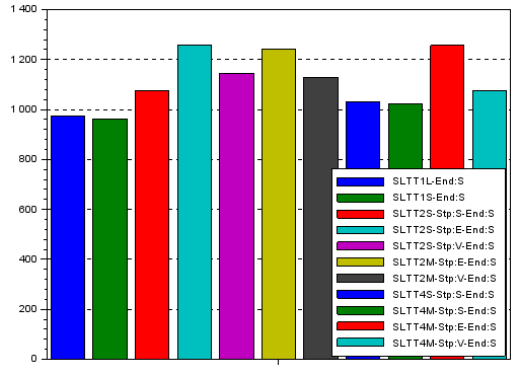

Figure 9 - Impeller revolution speed [*rpm*] predicted by the CFD model for the SLTT listed in Figure 4.

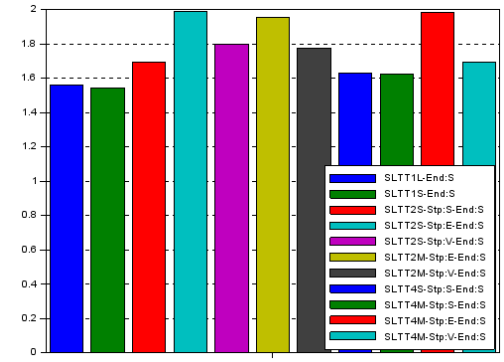

Figure 10 - Impeller torque [kNm] predicted by the CFD model for the SLTT listed in Figure 4.

Figure 12, in fact, presents the static merit coefficient C for the different analyzed stepped tunnel configurations, in addition to the two conventional straight tunnels. The coefficient is perhaps the most diffused way to measure the efficiency in producing bollard pull thrust by given a ducted propeller (Beveridge, 1972) and it is equal to:

$$C = \left(\frac{K_T}{\pi}\right)^{\frac{3}{2}} \frac{1}{K_Q} \qquad (2)$$

A maximum value C=2 is expected in ideal condition (no viscous losses, no expansion of the outflow).

The performance comparison of the various considered stepped long tunnel configurations, as can be inferred by the analysis of Figure 8, evidences that the highest value of total thrust is reached by the rounded stepped configurations, with a marked superiority of the SLTT4 configuration on the SLTT2E. This was expected since the larger diameter of the end sections of SLTT4 minimizes the inlet and outlet losses (lower average speed at the contracted inlet section) while increasing the suction force on the upstream step (*in.step*).

The flow rate (Figure 9) increases at the constant imposed thrust, for designs that achieve lower duct losses. Higher flow rate determines a higher advance ratio to the fixed pitch propeller that has to increase the speed to keep the assigned thrust. The torque requested by the Ka-4-70 duct propeller (Figure 10) comes as a consequence of the assigned thrust and the advance ratio calculated from the CFD simulation, from the characteristic curves given in Figure 5.

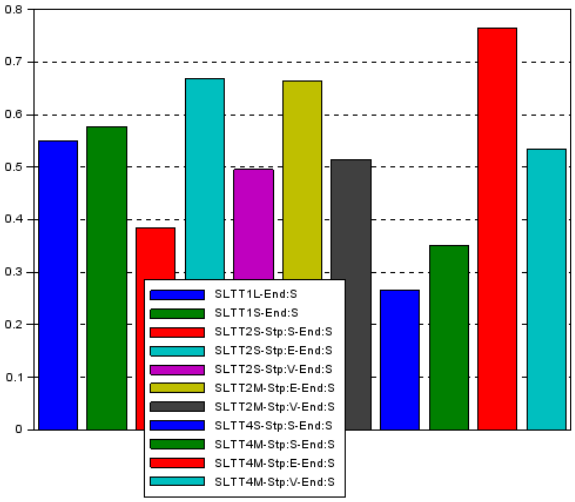

Figure 12 - Static merit coefficient *C* predicted by the CFD model for the SLTT listed in Figure 4.

Steady state viscous flow fields have been obtained for each of the tunnel configurations presented in section 3. Integration of pressure and shear forces on each surface allows to compute the total thrust as well as to compare the partial contribution of each new duct component to the total thrust. This comparison is given in the bar chart of Figure 14.

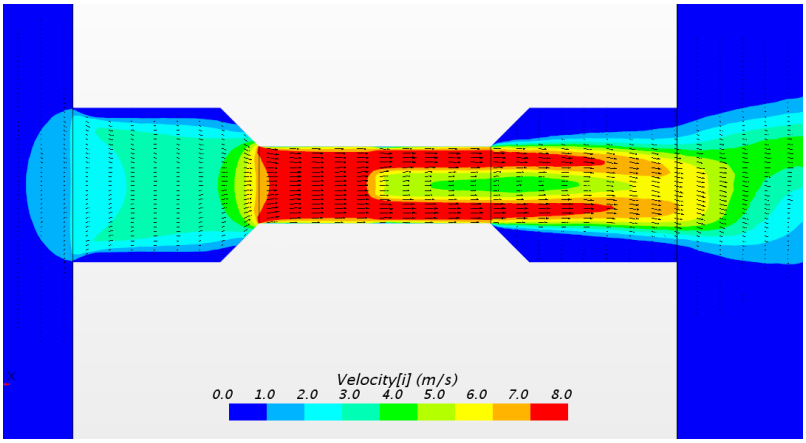

Figure 11 - Velocity flow field for SLTT4V-medium-OS

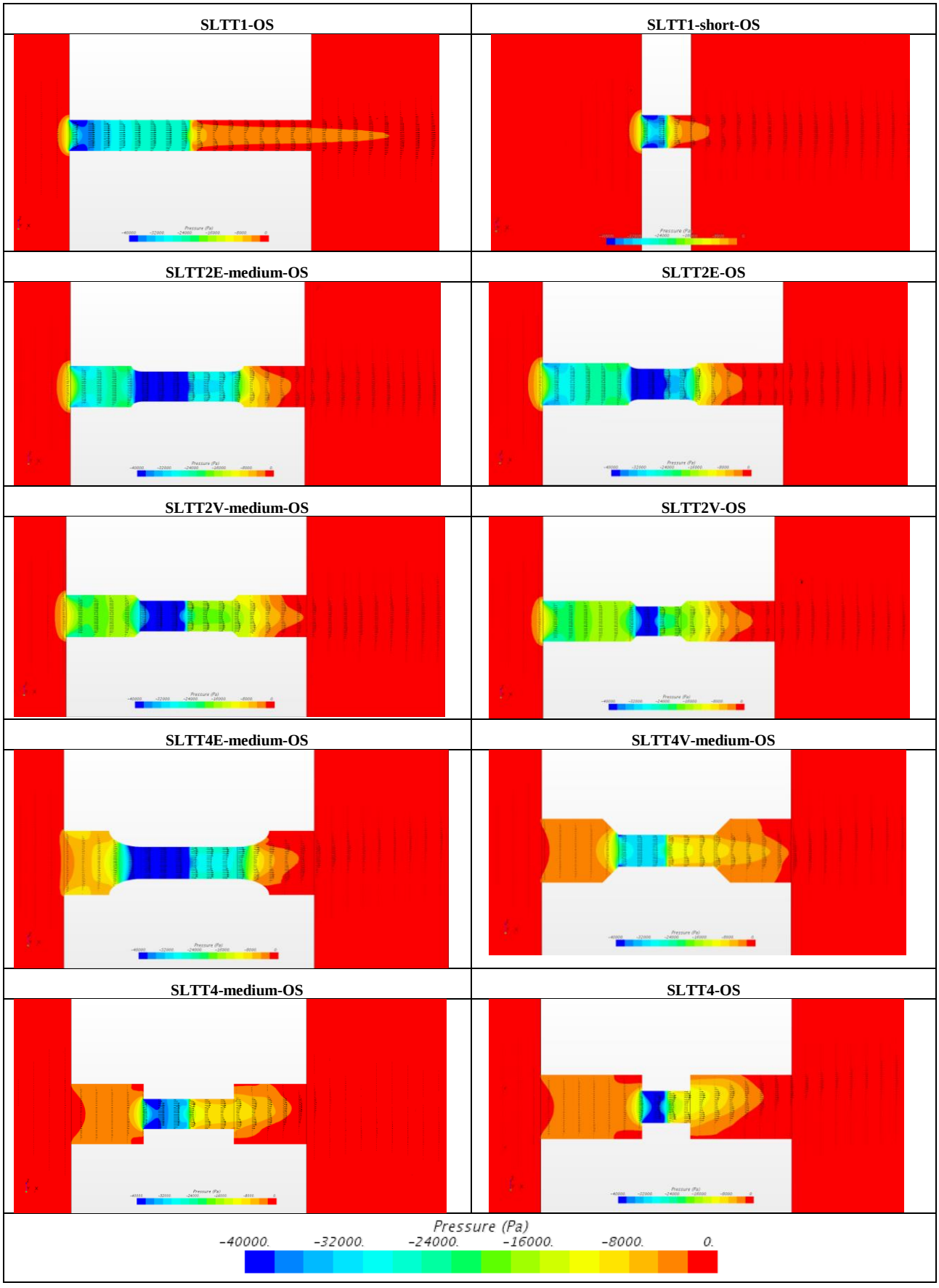

Figure 13 - Pressure distributions in a longitudinal (diametral) section of the investigated tunnel thrusters series. Color scale is the same for all graphs as reported at the bottom of the list.

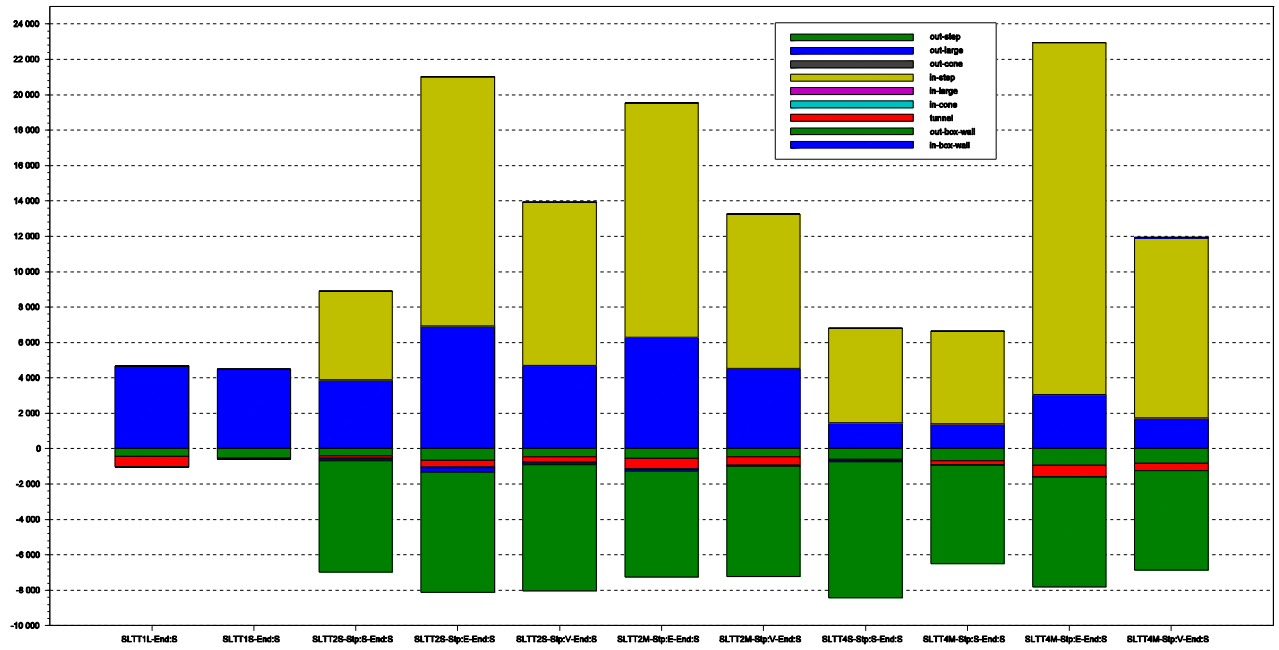

Figure 14 - Thrust production breakdown by each individual duct component of the considered stepped tunnel configurations (conventional constant diameter tunnels, SLTT1 are also included as first two cases). The contribution of the upstream step is noticeable and contrasted by the thrust deduction generated by the downstream step.

A careful analysis of the pressure distribution along the duct may indicate the location of the concentrated and distribution losses along the conduit. The computed pressure distribution on the longitudinal (diametral) section of the duct is presented in the Figure 13, for all considered cases.

As anticipated, the analysis of pressure distribution, evidences how the rounded step connections are able to minimize concentrated losses, while maximizing the suction pressure force on the *in.step* surface, which is the principal component of the total thrust produced by the duct system.

The larger inlet openings of stepped tunnel configurations are responsible for the reduction of the concentrated losses with respect to the smaller diameter inlet of the conventional tunnel. The analysis of the velocity field, as presented in Figure 11 for SLTT4V case, reveals how the conical step is effective in separating the jet flow exiting from the tunnel mid-section, at the same time avoiding the its reattachment onto the larger diameter section downstream. This contributes to the reduction of distributed (friction) losses in the *out.large* component of the duct.

Figure 14 presents the incremental contribution of each duct geometrical feature to the total produced thrust. Contributions creating useful thrust are piled up above the zero line, while negative contributions stacked below the zero reference line, represent a reduction of the total net thrust. It can be noted that, in the SLTT configurations, a major contribution to the total thrust is given by the *in.step* which is always subject to partial compensation of the negative thrust produced by the *out.step*.

The most efficient step connection, as already noted, is the rounded one, as the yellow (positive) taller bars in Figure 14 highlight.

Finally, for the CFD enthusiast: a close analysis of the pressure and velocity fields obtained throughout all computations and presented in the examples of Figure 11 and Figure 13, reveals an asymmetry of the flow exiting for the mid-section of the SLTT configuration. This asymmetry manifests as a periodic pressure and velocity fluctuation around a prevalent axial jet flow. It is obviously a consequence of the flow separation downstream of the stepped connection between the inner and the outer tunnel sections. Similar fluctuations have been measured for instance in the reattachment region of turbulent flows separating from a backward step (Kim et al., 1980). Also note that in the CFD simulations the outflow of the propeller disc is given both axial and rotational momentum. However, the RANSE simulations, presented in this paper, are indeed based on a 3D segregated steady flow solver. Steady simulations were continued over a large number of steps until optimal convergence (low residuals), but this flow unsteadiness continued to manifest. Due to the nature of the steady solver, this predicted unsteadiness must not be considered physical, but rather a virtual (numerical) phenomenon that is a symptom of a physical phenomenon (flow separation). The steady RANSE flow solver is meant to reach the steady state by virtual time step iterations. Future planned studies will repeat simulations with an Unsteady RANSE solver in order to confirm the average predicted forces coming from the steady model.

6 CONCLUSIONS

A new internal duct shape design is proposed for applications on long tunnel thrusters. The patented solution is based on a sudden radial step in duct diameter between the mid-section and the two end sections of the duct. Different alternative designs, obtained by varying the diameter difference (step height) and the shape of the stepped connection, while keeping the overall length, have been created and analyzed by means of high fidelity fully turbulent viscous flow simulations.

Results, obtained at constant impeller thrust, indicate that some designs are able to produce a considerably higher duct thrust and a higher static merit coefficient than the conventional tunnel thruster configuration. In particular, the rounded step configurations show static merit coefficient increase of about 23% (SLTT2E-short) to 40% (SLETT4E-medium), depending on the step height. This higher increase of efficiency is paired by a considerable increase of total thrust, amounting to 61% (SLTT2E-short) and 74% (SLETT4E-medium), with respect to the reference conventional long tunnel configuration.

Application potentials of the proposed technology are still to be completely unleashed, since the higher efficiency demonstrated by the stepped long tunnel configurations (L/D>4) has proven superior to conventional tunnel thruster having ideal tunnel lengths (2~3D) and same impeller diameter, by the CFD simulations presented in this study. Results of this study seem also to indicate the possibility to design tunnel configurations with smaller impeller diameters and the same efficiency and total thrust than current conventional installation. Future studies are planned to demonstrate evidences in this respect.

REFERENCES

Beveridge J. L. (1972). Design and Performance of Bow Thrusters, Marine Technology, **9**(4): 439-453.

Brizzolara E.B., Brizzolara S. (2016) Marine Tunnel Thruster. US patent US9376186B2. WIPO patent publication number WO2012/137144.

Brizzolara S., Villa D, Gaggero S (2008). A Systematic Comparison between RANSE and Panel Method for Propeller Analysis. 8th Int. Conf. on Hydrodynamics, ICHD 2008. Nantes, France, 1:289-302.

English J.W. (1963). The Design and Performance of Lateral Thrust Units for Ships. Transactions of RINA, **105**(3): 251-279.

Gaggero S., Savio L., Brizzolara S., Viviani M., Conti F., Ferrando M. (2009). Comparison of Experimental Measurements and Numerical Calculations for a Propeller in Axial Cylinder. First International Symposium on Marine Propulsors SMP'09, Trondheim, June 2009.

Kim, J., Kline, S. J., & Johnston, J. P. (1980). Investigation of a reattaching turbulent shear layer: flow over a backward-facing step. ASME J. Fluids Eng, 102(3), 302-308.

Ridley D. E. (1969). Effect of Tunnel Entrance Configuration on Thruster Performance, Marine Technology, **6**(2): 60-65.

Rodi W. 1991. "Experience with Two-Layer Models Combining the k-e Model with a One-Equation Model Near the Wall", 29th Aerospace Sciences Meeting, January 7-10, Reno, NV, AIAA 91-0216.

Stuntz, Jr., G. R. and Taylor, R. J. (1964). Some Aspects of Bow-Thruster Design, Trans. SNAME, **72**:336-373.

Taniguchi K., Watanabe K., Kasai H. (1966) Investigations into the Fundamental Characteristics and Operating Performances of Side Thruster, Mitsubishi Technical Bulletin n.35.

Van Manen J. D., Oosterveld M. W. C. (1966). Analysis of Ducted-Propeller Design, Trans. SNAME, **74**:522-562.

Villa D., Gaggero S., Brizzolara S. (2012). Ship Self-Propulsion with Different CFD Methods: from Actuator Disk to Viscous-Inviscid Unsteady Coupled Solvers. 10th Int. Conf. on Hydrodynamics, ICHD'12. St. Petersburg (Russia).

Yu C., Yang C. (2016). Study of Tunnel Thruster Performance and Flow by Quasi-Steady Reynolds-Averaged Navier-Stokes Simulations. J. Shanghai Jiaotong Univ. (Sci.), **21**(6): 662-671.